processes

MDPI

Article

Modelling the Behaviour of Pollutant Indicators in Activated Carbon Adsorption of Oil and Textile Effluents

Samia Rabet [1], Rachida Chemini [1], Gerhard Schäfer [2] and Farid Aiouache [3,*]

[1] Laboratory of Theoretical and Applied Fluid Mechanics (LMFTA), University of Sciences and Technology, Houari Boumediene (USTHB), BP 32, El-Allia, Bab-Ezzouar, Algiers 16111, Algeria; samia.rabet@usthb.dz (S.R.); rchemini@usthb.dz (R.C.)
[2] Institut Terre et Environnement de Strasbourg (ITES), UMR 7063 CNRS-Université de Strasbourg-ENGEES 5 rue René Descartes, F-67084 Strasbourg, France; schafer@unistra.fr
[3] School of Engineering, Lancaster University, Lancaster LA1 4YW, UK
* Correspondence: f.aiouache@lancaster.ac.uk

Abstract

Simulation studies of adsorption in complex effluents are challenging due to nonlinear interactions between sorbents, adsorbates and carrying flows. This study investigates effluents from oil and textile industries, characterised by their heavy metal content and chemical oxygen demand. It examines the process in a continuous-flow laboratory-scale adsorption system. Results were validated using process modelling based on mass and energy conservation, applied to an industrial adsorber. The model described surface sorption mechanisms on bioactivated carbon at the molecular level and predicted breakthrough curve profiles, integrated with Aspen Plus ® adsorption simulation under industrially relevant conditions. Experimental data and model predictions showed good agreement, with relative deviations ranging from 0.2% to 24.6%. Differences in adsorption capacities between oily and textile effluents highlighted the influence of coexisting constituents. At the same time, the varied behaviour of identical components supported the hypothesis of multifactorial effects in complex mixtures. The optimisation study, using Response Surface Methodology with a Central Composite design, evaluated factors such as bed height, feed rate, and adsorption cycle time, achieving enhanced removal efficiencies of 62% for chemical oxygen demand and 25% for suspended solids.

Keywords: pollution indicators behaviour; continuous adsorption; industrial wastewater; breakthrough curves prediction; response surface methodology

Academic Editor: Anna Wołowicz

Received: 17 November 2025
Revised: 18 December 2025
Accepted: 19 December 2025
Published: 24 December 2025

1. Introduction

According to the World Resources Institute, the global water crisis affects nearly a quarter of the world's population, partly due to excessive industrial water consumption [1]. The oil industry leads with an estimated global consumption of 2500 billion km^3 of water per year by 2025, followed by the textile industry, which consumes an estimated 93 billion km^3 per year. These industries are major contributors to industrial wastewater worldwide [1,2]. The effluents from the oil industry have a profound environmental impact due to increasing concentrations of persistent pollutants and toxic heavy metals [3]. Oil present in effluents forms a layer that prevents sunlight from reaching the leaves of aquatic plants and algae, thereby disrupting photosynthesis. This process depletes oxygen in the environment, leading to the collapse of the food chain and the disappearance of life forms in contaminated areas [4]. Oil discharges contain a variety of toxic substances, including gasoline, polycyclic aromatic

hydrocarbons (PAHs), heavy metals, and BTEX compounds (benzene, toluene, ethylbenzene, and xylenes). These substances, noted for their high solubility and stability in water, pose a significant threat to both the environment and human health. Exposure to these components can cause reproductive disorders, weaken immune systems, and increase the risk of cancer [5]. Benzene is particularly hazardous, as it can cause leukemia and bone marrow damage even at low concentrations (0.1 to 1 mg/L in water) [6]. Toluene and xylenes may result in central nervous system depression, liver and kidney damage, and developmental abnormalities. Ethylbenzene is associated with ototoxicity and endocrine disruption [7]. In contrast, textile wastewater contains substances such as heavy metals, hydrogen peroxide, acidic compounds (hydrochloric and sulfuric acids), and ammonia, which increase pH levels and oxygen demand, contributing to high biochemical oxygen demand (BOD) and chemical oxygen demand (COD) [7]. Azo dyes in textile wastewater reduce light penetration and inhibit photosynthesis. When degraded by bacteria or through metabolism, these dyes produce aniline, aromatic amines, and N-methylaniline. These non-biodegradable compounds can accumulate in fish, causing toxicity that is transmissible to humans and potentially leading, even at low doses, to bladder cancer, leukemia, and DNA damage [8].

According to Berez et al. (2016) and Manzoor and Sharma (2020), 12% of the 800,000 tons of pigments and dyes produced by the textile industry worldwide each year are lost in effluents during manufacturing processes, mainly discharged into surface waters [9–11]. The adoption of sustainable water management practices in these industries is repeatedly reported as crucial for mitigating environmental concerns related to global water conservation [12]. Among the various technical solutions for treating contaminated effluents, the adsorption process by activated carbon remains the most widely used technology due to its efficiency, economic returns, and flexibility in treating a range of effluent types and loads (i.e., organic and inorganic) [13–16]. Due to its large surface area (up to 1500 m^2/g) [17], and porous structure, this material exhibits high adsorption capacity to remove pollutants like azo dyes, BTEX, PAHs, heavy metals, and organics that resist biological degradation, and without sludge proliferation or excessive energy consumption [18]. Whereas other treatment technologies, such as advanced oxidation or membrane filtration, are limited in treating this type of wastewater due to incomplete pollutant removal or sensitivity to high salinity. Direct treatment by these processes may compromise their long-term proper functioning [19].

Advanced modelling of the adsorption process offers an alternative tool for predicting separation efficiency and reduces the need for laboratory experiments, which may not be affordable at various scales. It provides powerful pathways for addressing the complex, nonlinear dynamics of adsorption in the treatment of petroleum and textile wastewaters at reduced cost, supporting more efficient process optimisation [20]. Studies on modelling and process simulation of adsorption of multicomponent mixtures have mainly been conducted for gaseous-phase systems [21–26], whereas only a few have addressed aqueous mixtures [27–29]. The work of Xu et al. (2013) [27] provided a comprehensive overview of the models to describe the adsorption behaviour and column performance of the fixed-bed adsorption systems, including general rate models, the linear driving force (LDF), the wave propagation theory, the Clark model, Thomas model, among others, to predict the breakthrough curves at the exit of a fixed-bed. Their study also reproduced the fundamental concepts, hypotheses, and model development for mass transfer and isotherms, and discussed the extent of the assumptions and limitations of each model. The work of Leonavičienė et al. (2019) [28] employed a finite-volume and method-of-lines approach implemented in a MATLAB script using the ode15s solver to analyse the sensitivity of adsorption kinetics and equilibria models to adsorbent pore volume, surface diffusion, and mass transport. The approach contributed further to the formulation of a nonlinear partial

differential equation model of adsorption, which was linearised and normalised for the sensitivity analysis. Rodríguez-Narciso et al. (2021) [29] demonstrated the relevance of the approach based on a stochastic model while [30] used a rotating packed bed for modelling the adsorption of resorcinol, where the fundamentals of liquid hydrodynamics, mass transfer, and intraparticle diffusion kinetics helped predict the adsorption capacity under flexible operating conditions (i.e., high gravity factor, liquid spray density, pH, temperature, and inlet resorcinol concentration).

Recent advances in molecular simulation techniques have significantly enhanced understanding of dye adsorption mechanisms in wastewater, as demonstrated by Malloum et al. (2025) [31]. They studied the interactions between dyes and adsorbents, such as activated carbon and zeolites, using Molecular Dynamics Methods, Monte Carlo simulations and Density Functional Theory, and provided atomic-level insights into phenomena affecting adsorption capacity and selectivity. The integration of the molecular-level findings (i.e., hydrogen bonding and electrostatic interactions that govern absorption energies) and the macroscale models, such as the Bed Depth Service Time (BDST) breakthrough curves, helped in understanding the mechanisms associated with adsorption capacities and kinetics, prediction of performance, and optimisation of operational parameters for complex wastewater mixtures in the textile dye removal applications. At the macroscale, several articles investigated the prediction of pollution indicators using a modelling approach. Almadani (2023) investigated the breakthrough curves of COD, using a MATLAB code developed for the purpose, for a dissolved air flotation unit at the wastewater treatment site of an oil refinery [32]. The breakthrough curves provided further assessment of the model through sensitivity analyses of flow rate, inlet COD concentration, and bed height. The simulation tools offer an advantage in process prediction and optimisation. Still, the lack of pollution indicators and the scale-up for prediction limit their performance in terms of process operation, safety, and quality analysis. Monitoring and predicting the behaviour of pollution indicators during adsorption processes would help anticipate performance compliance with environmental standards, providing insight into system efficiency and environmental impact. The lack of a comprehensive framework to simulate and analyse the dynamic evolution of pollution indicators throughout the operational life cycle of separation systems was the driving force behind this work. A simplified 1D mathematical model that captures the influences of molecular diffusion and adsorption profiles of a multicomponent mixture is not straightforward to apply. The combination of solid properties, such as density, molecular radius, and molecular weight, would affect the molecular diffusion in the liquid film and through the pores. Fluid properties, such as density and viscosity, influence molecular diffusion in the liquid phase, thereby affecting overall adsorption rates. The dynamic evolution of pollution indicators in terms of COD, suspended solids (SS), turbidity, and pH as a function of time and height of the packed bed adsorber (herein the activated carbon) applied to effluents from two complex plants, oil and textile industries with nonlinear interactions between sorbents, is investigated using the adsorption simulation module (Adsim) of the commercial process simulation package Aspen Plus® V9 (AspenTech, Bedford, MA, USA) for process quality analysis, separation efficiency prediction and optimisation. The process is designed to operate continuously through a packed-bed column of activated carbon. The numerical model considers the relevance of kinetic characteristics and yield at adsorption equilibrium, helping to understand the complex interactions between sorbate and sorbent in realistic effluent mixtures and their impact on degree of saturation, regeneration time, and the efficiency of the packed bed column. It contributes to simulating and analysing the dynamic evolution of pollution indicators during dynamic adsorption. It uses the concepts of integration of mass and energy conservation with the LDF model, capturing multicomponent competition in

adsorption. An optimisation using the response surface methodology (RSM) with a central composite design is employed to assess the system's resilience and identify significant factors, accounting for complex interactions among process parameters [33–35].

2. Materials and Methods

2.1. Adsorbent

The chosen activated carbon was primarily derived from mature cypress heads, a type of non-recovered botanical waste, harvested locally during the dry summer season. The precursor material underwent a preparation process, starting with washing and followed by drying at 105 °C for 24 h. Following this, it was then precisely cut into 5 mm pieces and stored for further processing. Pure orthophosphoric acid served as an activating agent. The precursor material was impregnated with the acid solution at a mass impregnation ratio of unity for five hours. Subsequently, the activation was carried out at 100 °C under continuous stirring and in the absence of light. The precursor material was then subjected to a carbonisation process at 873 K for 4 h. The resulting activated carbon was washed with distilled water until the solution reached a neutral pH. It was then dried and stored for further analysis. The activated carbon characteristics are listed in Table 1 [12,36].

Table 1. Activated carbon characteristics.

Density (kg m^{-3})	Surface Area (BET) (m^2 g^{-1})	Pore Size (nm)	Pore Volume (cm^3g^{-1})	Porosity
550	379.51	≤39	0.204	0.65

The FTIR spectrum represented in Figure 1a of activated carbon reveals the presence of various functional groups, including aromatics, cyclohexanes, C=C double bonds, anhydride lactones, as well as O-C-O, methylene C-H and O-H groups. These groups selectively influence the surface adsorption properties of oily and textile mixtures. The FTIR analysis was carried out over a wavelength ranged between 600 and 4000 cm^{-1} using a Safas Monaco IR600 device, employing KBr pellets pressed at high pressure [37]. The XRD spectrum of activated carbon, shown in Figure 1b, displays two broad peaks at 2θ of 25° and 42°, which are characteristic of the partially ordered carbon structure. The broadness of these peaks confirms the predominantly amorphous nature of the activated carbon structure. X-ray diffraction (XRD) analyses were performed on an X-ray diffractometer over 2θ = 5–80° (step size 0.02°, time per step 0.5 s). Phase analysis and semi-quantitative estimation were carried out using HighScore Plus software (version 4.9, Malvern Panalytical, Malvern, UK) with the Reference Intensity Ratio (RIR) method from PDF-ICDD database files [37].

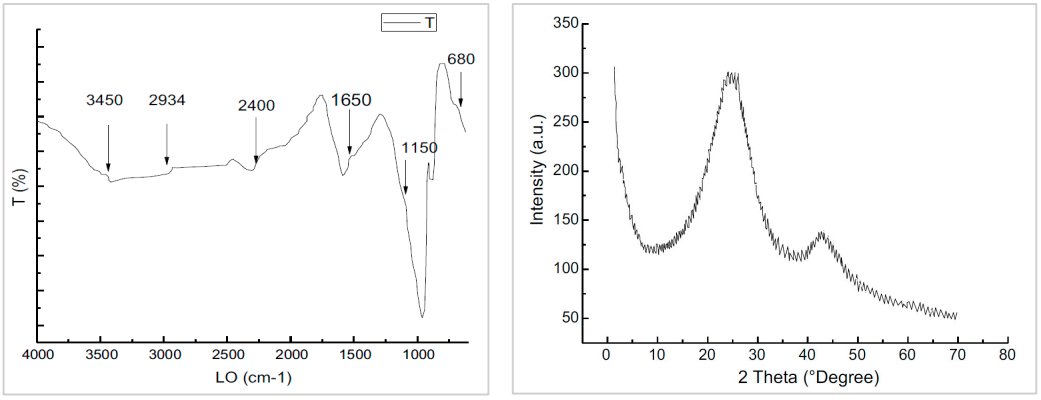

(**a**) (**b**)

Figure 1. (**a**) FT-IR spectrum of activated carbon, (**b**) X-ray diffraction analysis spectrum of activated carbon. Reproduced with permission from [37] © 2021 Springer Nature.

Figure 2a shows the scanning electron microscopy (SEM) images of the precursor before activation and calcination and of the activated carbon. The analysis was performed using a scanning electron microscope (FEI Quanta 650) [37]. The image of the activated carbon (Figure 2b) reveals the formation of irregularly shaped, non-uniformly sized cavities with a high specific surface area, compared to the precursor before activation and calcination. The pores are formed during heat treatment and chemical activation, resulting in a rough surface.

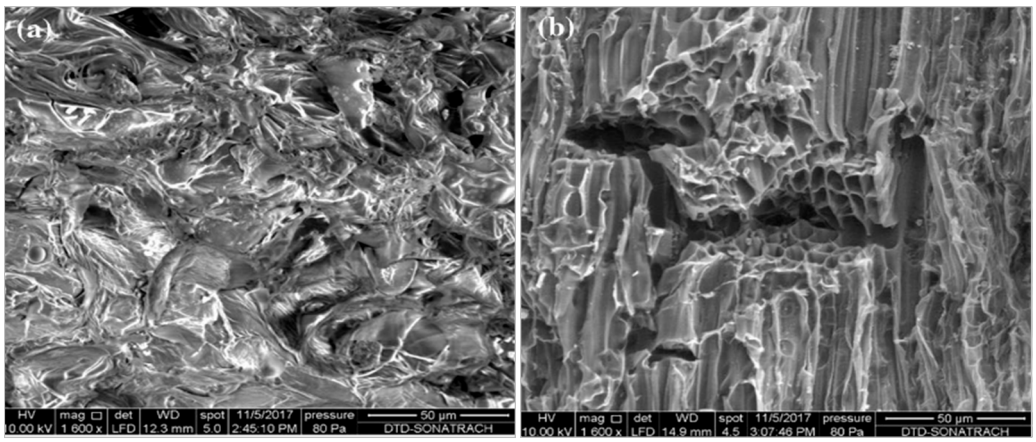

Figure 2. SEM of precursor (**a**) and activated carbon (**b**) (at 1600× magnification). Reproduced with permission from [37] © 2021 Springer Nature.

2.2. Numerical Model

2.2.1. Simulation Parameters

The adsorption simulation of oil and textile effluents was conducted in a single adsorption column containing a fixed bed of activated carbon. The oil wastewater was obtained from the oil recovery station in Tin Fouyé Tabankort region (Sonatrach Ltd., Illizi, Algeria), and the textile wastewater was recovered from a local textile production unit in Batna region (Cotitex Ltd., Batna, Algeria). The case study represents a laboratory-scale treatment of oil or textile effluents at a flow rate of 1.5 litres per hour. The first step was to create the process flow diagram of the simulation model, as shown in Figure 3. The characteristics of the adsorption column and the feed composition are illustrated in Tables 2 and 3, respectively [36]. The column dimensions were chosen based on the experimental results [36]. The height-to-diameter ratio was approximately 1.5, while the ratio of bed diameter to activated carbon particle diameter was greater than 100, ensuring negligible effects at the bed entrance and walls and enabling uniform mixing throughout the bed height, thereby enabling the use of a one-dimensional fluid flow model.

Table 2. Characteristics of the adsorption column.

Parameter	Value
Height (m)	0.15
Diameter (m)	0.1
Flow rate Q (L h^{-1})	1.5
Porosity of the adsorption bed ε [-]	0.44
Cycle time t (min)	50
Temperature (°C)	25
Pressure (bar)	1

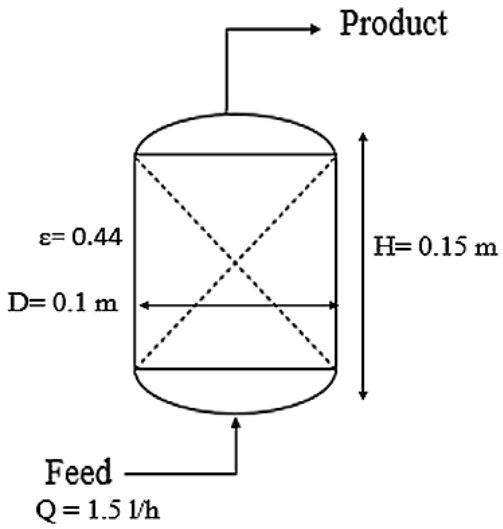

Figure 3. The simulated adsorption column.

Table 3. Characteristics of the oil and textile effluents [36].

Parameters	Oil Effluent	Textile Effluent
pH	6.5	10.6
Colour (PtCo unit)	-	500
COD (mg L^{-1})	5650	865
Suspended solids (mg L^{-1})	1648	122
Turbidity (FAU)	1863	234
TOC (mg L^{-1})	1229	345.5
Cl (mg L^{-1})	9	1.55 10^{3}
Ca (mg L^{-1})	36.07	36.1
Fe (mg L^{-1})	2.46	-
Mn (mg L^{-1})	75.8	5.29 $\times 10^{-5}$
Cd (mg L^{-1})	4.70 10^{-4}	11.99 $\times$ 10^{-4}
Cr (mg L^{-1})	3.58 $\times$ 10^{-4}	1.41 $\times$ 10^{-3}
Cu (mg L^{-1})	9.85 $\times$ 10^{-4}	1.91 $\times 10^{-3}$
Ni (mg L^{-1})	7.50 $\times$ 10^{-6}	4.21 $\times 10^{-3}$
Pb (mg L^{-1})	4.84 $\times$ 10^{-3}	--
Zn (mg L^{-1})	1.00 $\times$ 10^{-3}	8.17 $\times$ 10^{-3}
Fluid density (kg m^{-3})	987.17	991.26
Dynamic viscosity (Pa s)	1.79 $\times$ 10^{-3}	9.83 $\times$ 10^{-4}

The analytical methods and the instruments for the characterisation of wastewaters are illustrated in Table 4 [36].

Table 4. Key physical parameters and corresponding analytical methods.

Parameter	Method	Instrument
pH	Hydrogen ion concentration	pH meter WTW Inlab 735 (WTW, Weilheim, Germany)
Conductivity	Electrical conduction electrodes	Conductivity meter HACH HQ40d (Hach, Loveland, CO, USA)
COD	Potassium dichromate	Spectrophotometer HACH DR1900 (Hach, Loveland, CO, USA)
BOD5	5-day incubation at 20 °C	Incubator Oxitop IS 200 WTW (WTW, Weilheim, Germany)

Table 4. *Cont.*

Parameter	Method	Instrument
Colour	Platinum-cobalt (Pt/Co)	Spectrophotometer HACH DR1900 (Hach, Loveland, CO, USA)
Turbidity	Formazine Attenuation Unit (FAU)	Turbidimeter HACH 2100 N (Hach, Loveland, CO, USA)
TSS	45 µm filtration	HACH 45 µm filter (Hach, Loveland, CO, USA)
TOC	High-temperature combustion	Skalar Formac HT-I TOC Analyser (Skalar, Breda, The Netherlands)
Hydrocarbons	Hexane extraction + GC	GC Clarus 580 PerkinElmer (PerkinElmer, Waltham, MA, USA)
Heavy metals	Plasma spectrometry	ICP Optima 8000 PerkinElmer (PerkinElmer, Waltham, MA, USA)
Cations/Anions	Ion chromatography	ICS 5000+ DC Thermo Scientific (Thermo Scientific, Waltham, MA, USA)

2.2.2. Mathematical Models

Mass Conservation

A macroscopic description approach representing the effective behaviour of the porous media was used, based on the representative elementary volume concept (Bear, 1972) [38] and a one-dimensional mass balance model for a given species i transported in the water phase across a packed bed under steady-state flow conditions [16,39]. The velocity in the bed, U, was determined considering a non-dispersive plug-flow model of constant residence time, t

$$t = \frac{V_v}{UA} \tag{1}$$

where V_v is the void volume of the adsorption column, and A is the cross-sectional area of the bed. The mass balance then accounts for dispersion, advection, and adsorption. As expressed by Equation (2).

$$\frac{\partial C_i}{\partial t} = D_{e,i}\frac{\partial^2 C_i}{\partial z^2} - U\frac{\partial C_i}{\partial z} + \left(\frac{1-\varepsilon}{\varepsilon}\right)\frac{\partial q_i}{\partial t} \tag{2}$$

The mass transfer from the water phase to the solid phase was described by the mass conservation condition at the microscopic scale, given by the Linear Driving Force model [23,24,40–42].

$$\frac{\partial q_i}{\partial t} = k_{LDF}\,(q_i^* - \overline{q_t}) \tag{3}$$

The linear driving force mass transfer coefficient k_{LDF} is given by (Equation (4)) [21].

$$\frac{1}{k_{LDF}} = \left[\frac{r_p}{3\frac{Sh_i.D_{mi}}{2r_p}} + \frac{r_p^2}{15\varepsilon_P D_{eff}}\right]\frac{q_i^*\rho_p}{c_i} \tag{4}$$

The film mass transfer coefficient and the effective diffusion coefficient in the pores are given by Equations (5) and (6), respectively.

$$D_{mi} = \frac{KT}{6\pi r_i \mu_f} \tag{5}$$

$$D_{eff} = D_{S0} \frac{\partial \ln c_i^*}{\partial \ln q_i^*} \quad (6)$$

The multi-component Langmuir isotherm model, giving the equilibrium adsorbate concentration in the solid phase as a function of the concentration of the different constituents in the liquid phase [43], was selected with reference to the experimental results of a methylene blue and yellow S2FLR Bezathren on the same activated carbon, indicating monolayer adsorption [36].

$$q_i^* = \frac{q_{max} b_i C_i}{1 + \sum_{j=1}^{j=N} b_j C_j} = \frac{b_i' C_i}{1 + \sum_{j=1}^{j=N} b_j C_j} \quad (7)$$

The axial dispersion coefficient, which reflects deviations from plug flow due to hydrodynamic effects, was estimated using the correlation developed by Edwards and Richardson (1969) [44].

$$D_{e,i} = 0.73 D_{mi} + \frac{U\, r_p}{1 + \frac{9.7\, D_{mi}}{2\, U\, r_p}} \quad (8)$$

Energy Conservation

The principle of energy conservation, which describes the evolution of temperature as a function of time and space, is given by the heat balance model [39].

$$\rho_l \frac{\partial (cp_{li} T)}{\partial t} = k \frac{\partial^2 T}{\partial z^2} - \rho_l U \frac{\partial (cp_{li} T)}{\partial z} - \frac{1-\varepsilon}{\varepsilon} \left(\sum_i \Delta H_{ads,i,T_{ref}} + \rho_i cp_i \Delta T \right) \frac{\partial q_i}{\partial t} \quad (9)$$

2.2.3. Assumptions

A set of assumptions was used to solve the mathematical models, including a unidirectional mass-transfer model along the vertical axis, negligible energy exchange with the surrounding medium (i.e., pseudo-adiabatic operation), a constant average pore velocity along the column, and constant heat and mass transfer coefficients. Table 5 summarises the Langmuir isotherm parameters b_i and b_j used in the ADSIM module, as described in Equation (7), and the adsorption enthalpy. ΔH_{ads} of all modelled constituents.

Table 5. ADSIM's isotherm parameters b_i and b_j and the adsorption enthalpy [36].

Constituent	Water	TOC	Ca	Cl	Cd	Cr	Cu	Fe	COD	Mn	Ni	Pb
b_i (L g^{-1})	0.009	0.012	0.018	0.042	0.007	0.027	0.018	0.020	1.4×10^{-4}	0.021	0.018	0.006
b_j (L mg^{-1})	2.34	5.00	2.00	4.00	6.00	3.45	2.65	6.00	2.00	3.56	5.76	4.00
ΔH_{ads} (J.mol^{-1})	−68.26	−8.28	−129.65	−55.68	−29.57	−1.23	−10	−83.48	−110.10	−1.42	−10	−42.44

2.2.4. Spatial and Temporal Discretisation of the Model Domains

The mass transport equation (Equation (2)) and energy equation (Equation (9)) were solved simultaneously by the method of lines. To ensure stable solutions with reduced oscillations, an upstream fine difference scheme, UDS1, was embedded in Aspen Plus. The column was discretised into 20 equal cells of 0.0075 m height to study the spatial variation in concentration and heat. The overall simulation time was set to 50 min, corresponding to the cycle time [36], using a constant time step of 2.5 min. The increase in the number of nodes allowed for a variation of 10^{-9} for results with limited parameters (Ca, Zn, and Fe), indicating convergence stability of the discretisation approach. The physical properties of the components were estimated through the property database embedded in Aspen Plus. The model's input parameters are listed in Table 3. The one-dimensional mass and energy conservation models, including mass transfer kinetics between the liquid and solid phases

and the adsorption isotherm model, produced dynamic solutions of concentration trends along the height of the fixed-bed column.

2.2.5. Initial and Boundary Conditions

Table 6 summarises the boundary and initial conditions used to predict any missing thermodynamic property. The non-random two-liquid model (NRTL) was adopted to account for the non-ideal behaviour of ionic species, particularly due to strong electrostatic interactions that inhibit ideal mixing.

Table 6. Initial and boundary conditions for mass transfer and heat transfer.

Initial and Boundary Conditions		Mass Transfer		Heat Transfer
t = 0		$C = 0$	$q = 0$	$T = T_0$
t > 0	z = 0	$C = C_0$	$q = 0$	$T = T_0$
t > 0	z = H	$\frac{dC}{dt} = 0$	$\frac{dq}{dt} = 0$	$\frac{dT}{dz} = 0$

3. Results and Discussion

3.1. Temperature Behaviour in the Treatment of Oil and Textile Effluents

Preliminary calculations based on the energy equation (Equation (9)) indicated a slight increase in the adsorbent temperature at the column outlet, of less than 1 °C, for both oil and textile effluents. This is primarily due to the column's small size. This observation indicates the system's thermal stability and the influence of column size on its temperature behaviour.

3.2. Oil Effluent

3.2.1. Model Input Parameters: Diffusion Coefficients

The input parameters used in the numerical model are listed in Table 7 and calculated using Equations (4)–(6).

Table 7. Mass transfer coefficients used in the simulation of the oil effluents, the molecular radius r_i, the molecular diffusion coefficient through the liquid film D_{mi}, the diffusion coefficient in activated carbon pores D_s, and the linear driving force coefficient k_{LDF}.

Constituent	TOC	Ca	Cl	Cd	Cr	Cu	Mn	Zn	Ni	Pb	Fe
r_i (pm)	1400	180	100	215	128	128	140	138	135	180	140
D_{mi} (10^{-6} m^2s^{-1})	0.87	12.56	16.04	7.86	8.71	9.03	8.71	6.10	8.96	7.72	8.71
D_s (10^{-6} m^2s^{-1})	1.26	12.70	11.13	6.19	6.53	6.17	7.06	3.19	5.02	5.91	6.53
k_{LDF} (10^{-6} s^{-1})	6.67	44.35	17.8	7.92	6.90	6.71	8.48	4.16	6.06	0.25	6.18

The results indicate that the molecular radius and molecular weight are significant in controlling diffusion through the liquid film, where the specific surface area of the molecule increases the resistance to mass transfer. The molecules in the oil effluent were found to be more diffusive in the liquid film than in the pores, where the fluid velocity in the packed porous media accelerated particle movement in the liquid film. The initial concentration also had a significant effect on molecular diffusion in the liquid film and the pores, due to the large mass transfer gradient. Ge-Jia et al. (2025) [45] emphasised the importance of the initial concentration on the diffusion parameters. A high initial concentration led to faster external mass transfer and increased the relevance of the adsorption kinetics. The results indicate that the species of the smallest molecular radius (e.g., calcium and chlorine), with significant concentrations, are the most diffused, with k_{LDF} values of 4.45×10^{-6} s^{-1} and 1.78×10^{-6} s^{-1}, respectively. This aligns with the work of Satyam and Patra (2024) [46],

who demonstrated that smaller molecules exhibit greater accessibility to adsorbent pores, thereby enhancing intraparticle diffusion to the adsorbent surface.

3.2.2. Spatial Distribution of Constituents of the Oil Effluent

The evolution of the computed relative concentrations (C/C_0) of all constituents of the oil effluent as a function of the bed height, achieved after 50 min, is shown in Figure 4.

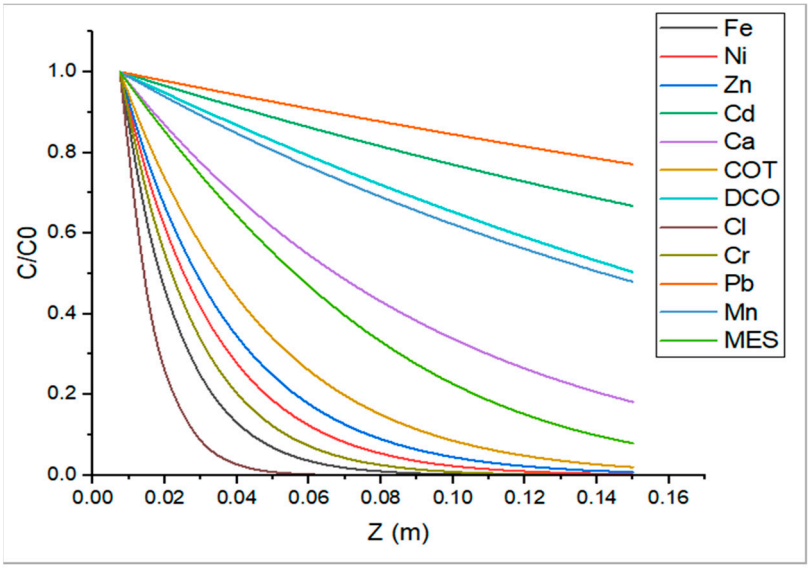

Figure 4. Computed relative concentrations (C/C_0) of all constituents of the oil effluent as a function of the vertical coordinate. C_0 corresponds to the concentration of each constituent at the inlet of the column (z = 0).

A total elimination of heavy metals (Cr, Fe, Ni, Zn), chlorine, and Total organic carbon (TOC) is observed at a height of 0.14 m. Eliminations of approximately 92% of suspended solids (SS), 43% of COD, and roughly 82% and 33% for calcium and cadmium, respectively, were achieved. The difference in the elimination rate is mainly driven by mass transfer kinetics, as reflected in the values of the relevant k_{LDF} (i.e., an acceleration of elimination at higher values) [30,47] and the concentration gradients. The k_{LDF} coefficient for the most adsorbed chlorine species of 1.5×10^{-5} s^{-1} is approximately double the values of manganese (8.48×10^{-6} s^{-1}) and cadmium (7.6×10^{-6} s^{-1}) caused by the solid-molecule characteristics (size, molecular weight, molecular diffusivity and density).

3.2.3. Breakthrough Curves of the Oil Effluent

The breakthrough curves for three selected constituents, expressed as the relative concentration ratio (C/C_0), are shown in Figure 5 at different locations along the column. Figures 5a, 5b and 5c illustrate the breakthrough curves of COD, suspended solids SS, and lead Pb, respectively.

The results indicate that the adsorption column reached saturation at 50.4% in COD, 7.9% in suspended solids, and 77% in lead after a 50-min adsorption cycle. A flat breakthrough curve indicates lower saturation and significant mass transfer resistance, depending on the mass transfer coefficient and bed length. At early bed height, the curve rises sharply, indicating adsorption at reduced resistance and a narrower mass-transfer zone. A rapid intraparticle diffusion control drives it and confirms (i) a fast initial kinetics earlier to the emergence of the pore diffusion limitations, matching multicomponent studies where the sharp curves represent optimal performance; (ii) a rapid external film diffusion before intraparticle limitations [48]. The bed was mostly saturated with lead despite its low

initial concentration, which was mainly compensated by its affinity for activated carbon (Figures 4 and 5).

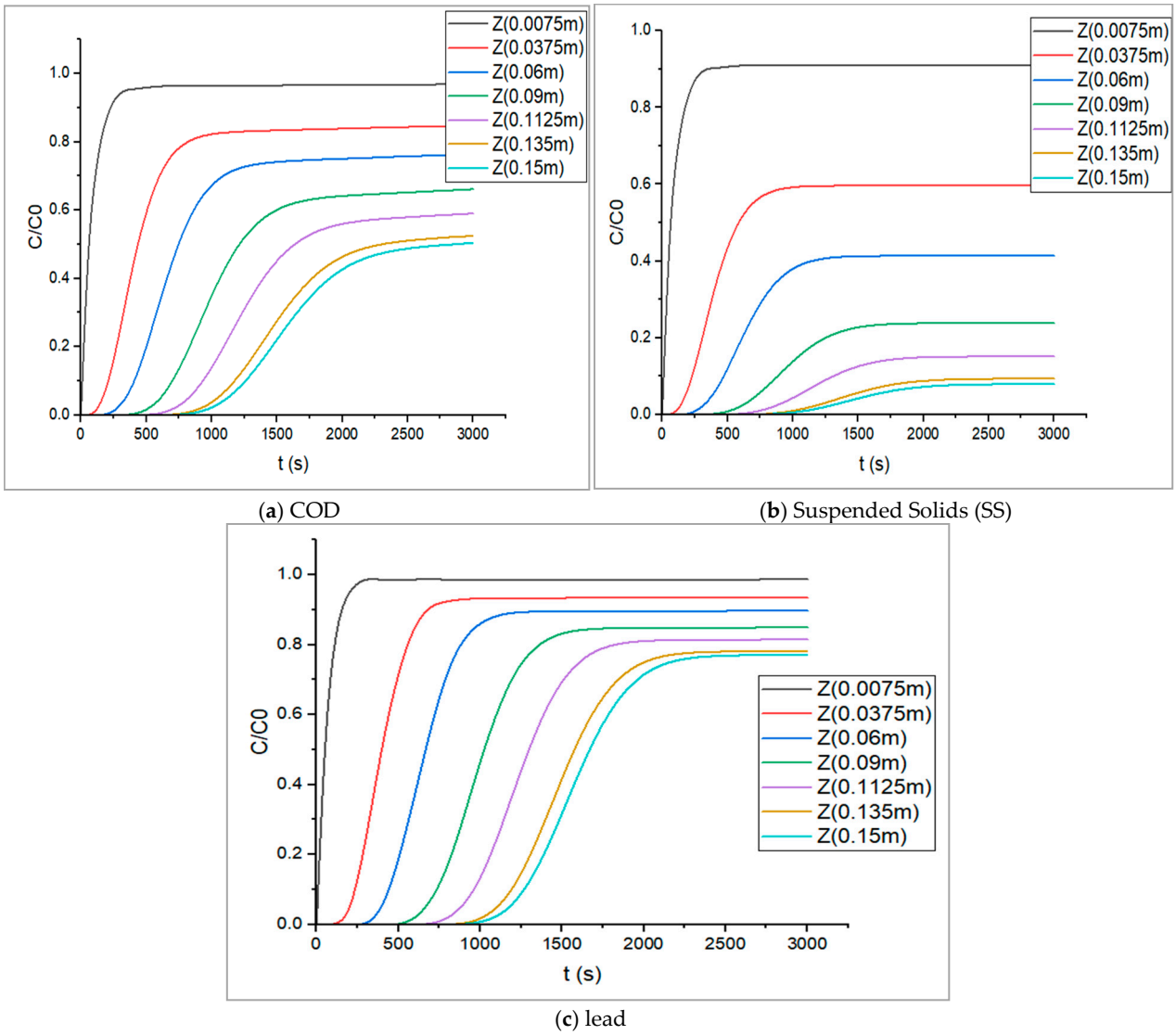

(**a**) COD (**b**) Suspended Solids (SS)

(**c**) lead

Figure 5. Breakthrough curves for COD (**a**), Suspended Solids (**b**), and lead (**c**) in oil effluents.

The simulation results for oil effluent adsorption, including chemical pollution indicators and relevant deviation percentages for the treated effluent recovered at the outlet of the adsorption column, are shown in Table 8.

Table 8. Experimental and computed results of the oil effluent.

Parameters	Treated Oil Effluent		Deviation (%)
	Experimental	Simulated	
pH	12	9.05	24.6
COD (mg L^{-1})	3219	2847.03	11.5
Turbidity (FAU)	147	146.66	0.2
Suspended solids (mg L^{-1})	139	130.56	6.0

The results demonstrate the effectiveness of the used model in predicting turbidity and suspended solids after a 50-min adsorption cycle, under the operating conditions specified in Table 2. The relative deviations between the experimentally determined values and those obtained by modelling the parameters turbidity and suspended solids were 0.2% and 6.1%, respectively. The COD is 11.6%, while the pH is 6.4%.

3.3. Textile Effluent

3.3.1. Mass Transfer Coefficient Input Data

The mass transfer coefficient and diffusivities in pores and films of the textile effluent used in the present study to predict external and internal mass transfer resistances are summarised in Table 9 and calculated using Equations (4)–(6).

Table 9. Mass transfer coefficients used in the simulations of the textile effluent: the molecular diffusion coefficient through the liquid film D_{mi}, the diffusion coefficient in activated carbon pores D_s, and the linear driving force coefficient k_{LDF}.

Constituent	TOC	Ca	Cl	Cd	Cr	Cu	Mn	Zn	Ni
D_{mi} (10^9 cm^{2}s^{-1})	0.171	1.33	2.4	1.117	1.877	1.877	1.716	1.741	1.78
D_s (10^9 cm^{2}s^{-1})	0.19	2.35	4.56	1	1.21	0.97	0.98	2.91	0.28
k_{LDF} (10^6 s^{-1})	0.47	4.41	43.3	1.54	2.67	2.36	1.41	3.17	0.87

As in the case of oil effluent, the diffusivity, molecular radius, molecular weight, and initial concentration all influence diffusion through the liquid film and in the pores. The chlorine molecule diffused more rapidly in the textile effluent, which has the smallest radius and highest concentration, with k_{LDF} of 44.3 × 10^{-6} s^{-1}. Calcium, chlorine, and zinc diffused faster in the pores than in the liquid film, and cadmium, chromium, copper, manganese, and nickel, promoted by the concentration gradient, diffused faster in the fluid film than in the pores.

3.3.2. Spatial Distribution of Constituents of the Textile Effluent

The evolution of the computed relative concentrations (C/C_0) of all constituents of the textile effluent as a function of the bed height, achieved after 50 min, is shown in Figure 6.

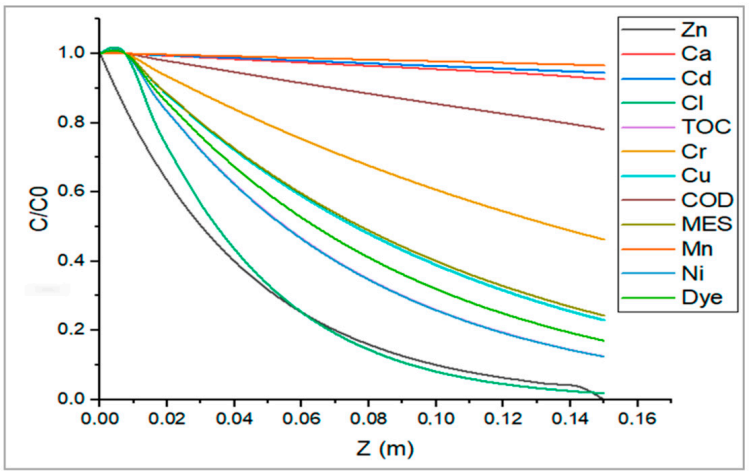

Figure 6. Computed relative concentrations (C/C_0) of all constituents of the textile effluent as a function of the vertical coordinate. C_0 corresponds to the concentration of each constituent at the inlet of the column (z = 0).

The results show complete removal of zinc, with traces of chlorine remaining at the end of the adsorption cycle. Elimination of 80% in colour, 81% in suspended solids, 83% in TOC, and 70% in copper is observed. Column saturation is noted for cadmium, manganese, and calcium. There is, however, a notable deficiency in COD removal with only 19% separation effectiveness compared to the oil effluent, mainly caused by the initial concentration of organic and inorganic matters present in the petroleum (5650 mg L^{-1}) and textile (919 mg L^{-1}) discharges, which are proportional to the concentration gradient and final saturations [49]. For instance, the competition between molecules on the active adsorbent sites in the cases of chlorine and organic and inorganic matters (COD), where chlorine is more concentrated (1529.6 mg L^{-1}) and consequently was adsorbed more quickly. Furthermore, the molecule size has a significant effect [50]. The results of Bayuo et al. (2023) [51] demonstrate that metals with higher affinity saturate high-energy sites first, leading to faster breakthrough of competing ions and corresponding to the observed adsorption rates. This competitive behaviour indicates the complex impact of ion size, charge density, and hydration on site occupancy and the overall efficiency of the process.

3.3.3. Breakthrough Curves of the Textile Effluent

Breakthrough curves for the two parameters, COD and suspended solids, were used to depict the dynamics of bed saturation at different column elevations due to chemical pollution from the textile effluent.

The adsorption column was saturated with 78% COD and 28% suspended solids. The manganese breakthrough curve was added to illustrate the complete saturation of the adsorption column. There is a linear relationship between the molecule geometry and the saturation extension, as an adsorption indicator. In the three cases, the slope of the breakthrough curve became flatter at an extended bed length, indicating an extension of the equilibrium zone and a reduction in the mass transfer zone, mainly due to intraparticle diffusion and concentration gradients.

As shown in Figures 6 and 7, the behaviour of molecules differs. Some molecules are quickly saturated, and others are less saturated, depending on their affinity and selectivity to activated carbon [50]. There was also clear competition among adsorbates, which influenced the quality of separation at a given time and, by inference, the bed height. The performance of molecules in oil and textile effluents varies significantly for some species. It is influenced by the physicochemical characteristics of these effluents, such as density, viscosity, and initial concentrations.

The simulation results for textile effluent adsorption, including chemical pollution indicators and their relative deviations, are illustrated in Table 10.

Table 10. Experimental and simulated results of the textile effluent.

Parameter	Treated Textile Effluent		Deviation (%)
	Experimental	Simulated	
pH	12	11.34	5.49
COD (mg L^{-1})	700	675.83	3.45
Turbidity (FAU)	77	71.38	7.29
Suspended Solids SS (mg L^{-1})	35	37.19	6.27
Colour (PtCo Unit)	98	88.68	9.50

The results show good predictions at the outlet section for almost all parameters, with deviation percentages ranging from 3.45% to 9.50%, and even better pH predictions for the textile effluent, which is less viscous and more diluted.

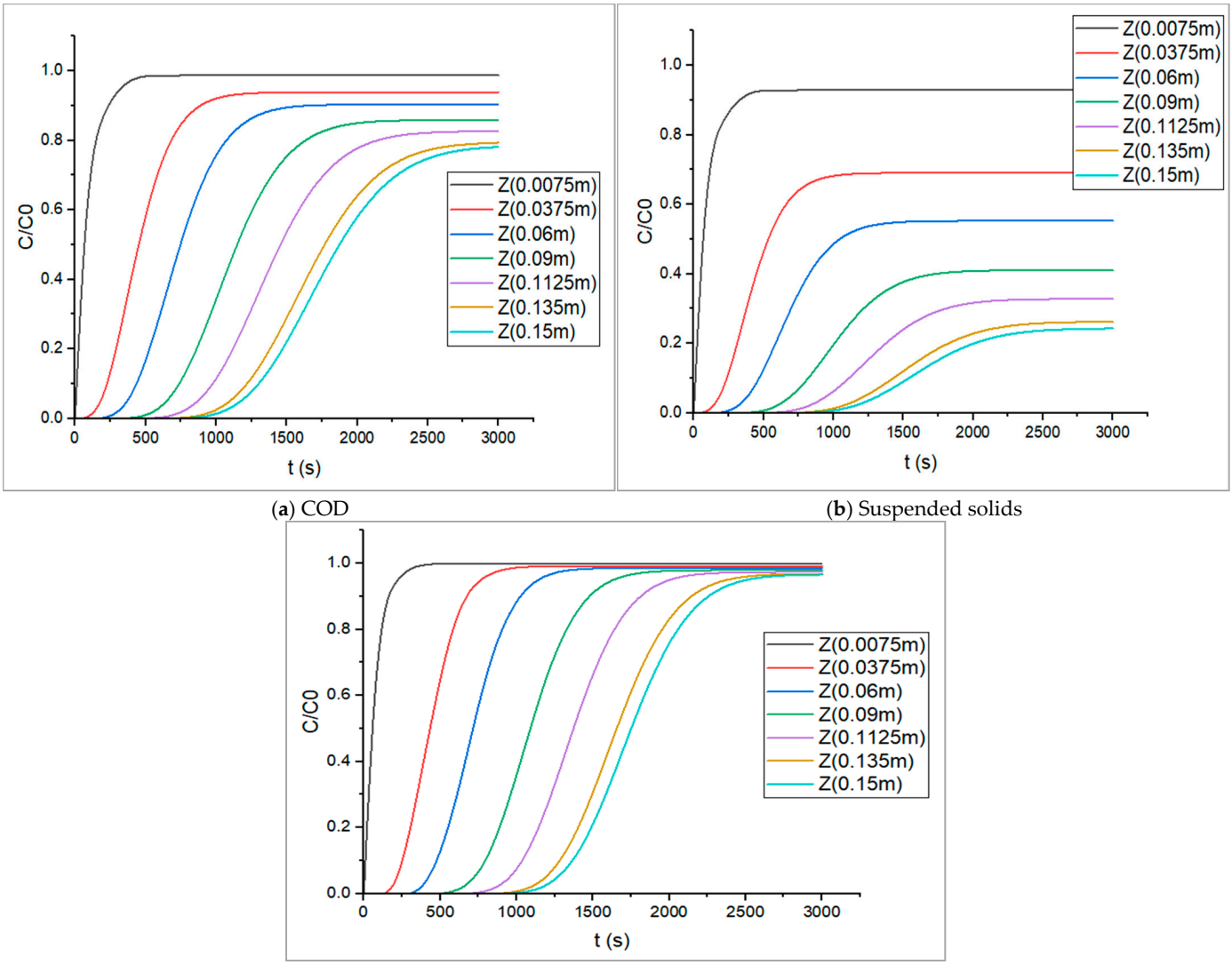

(**a**) COD (**b**) Suspended solids

(**c**) Manganese

Figure 7. Breakthrough curves for COD (**a**), Suspended Solids (**b**), and Manganese (**c**) in the textile effluent.

3.3.4. Optimisation of the Adsorption in the Textile Adsorption Column

The previous results indicated a wide range of values, including a low COD removal rate of 19% and a moderate suspended solids removal rate of 71.3% in textile effluent, as well as a significant impact of the column's adsorptive height on the breakthrough curves of COD at different elevations. Further optimisation studies were then required to assess the column efficiency more quantitatively. The Design of Experiments (DOE) approach, using JMP8 software V8 (JMP, SAS company, Cary, NC, USA), was used to further optimise the operating key factor parameters. The Response Surface Methodology (RSM) with Central Composite Design (CCD) was employed by constructing a matrix of 16 trials, with two trials at the centre, by varying three operating factors: bed height, feed rate, and adsorption cycle time, at three levels, as represented in Table 11.

The statistical analysis results indicate a good fit between the actual and predicted values, with correlation coefficients (R^2) of 0.95 for COD and 0.98 for suspended solids. The probability values were low, indicating the model's significance: p values of 0.001 and 0.0117 for suspended solids and COD, respectively.

Table 11. Factor levels for the selection of key operating factors.

Operating Key Factors	Symbol	Levels Values		
		−1	**0**	**+1**
Bed height (m)	X_1	0.10	0.15	0.20
Flow rate Q (L h^{-1})	X_2	1	1.5	2
Cycle time (min)	X_3	20	50	80

The analysis of variance (ANOVA) and Student's test presented in Table 12 helped adjust the model given by Equation (10). By studying the hypothesis (H_0) for each coefficient and each group, the second-order interactions were eliminated because they were not statistically significant. This test was carried out at the significance level of risk ($\alpha = 0.05$) by comparing the Fisher calculated value with the Fisher critical value ($F_{cal} = 9.36 > F_{crit} = 4.74$), indicating a statistically significant difference among the groups. The student t-values for the second-order variables were less than the critical value ($t_{crit} = 2.57$), indicating no influence on the response.

$$COD\ removal(\%) = 31.34 + 14X_1 - 23.24X_2 - 24.64X_3 - 13.15X_1X_2X_3 \quad (10)$$

Table 12. ANOVA analysis for COD and suspended solids models.

Component	Source	DF	Sum of Squares	Mean Square	F Ratio
COD	Model	10	17,781.82	1778.18	9.36
	Error	5	948.94	189.79	Prob. > F
	Total	15	18,730.76	-	0.0117 *
Suspended solids	Model	10	7165.05	716.50	26.51
	Error	5	135.10	27.02	Prob. > F
	Total	15	7300.16	-	0.001 *

Note: * denotes statistical significance at $p \leq 0.05$.

Figure 8 shows the 3D surface plots of COD removal as a function of bed height with the flow rate (Figure 8a), flow rate with time (Figure 8b), and bed height with time (Figure 8c). The results show that bed height has a positive effect of +14.5 on COD removal, with an optimum value of +0.3 (0.165 m). However, the fluid flow rate and the adsorption cycle time had adverse effects of −23.2 and −24.5, respectively, on COD removal and the optimum coordinate observed on the 3D surface plots was located at a level of −1. The negative value of −13.5 for the interaction of the three parameters ($X_1X_2X_3$) indicates an antagonistic effect at high values of bed height (X_1), flow rate (X_2), and adsorption cycle time (X_3), resulting in a 13.5% decrease in COD removal due to the activated carbon saturation.

Analysis of variance (ANOVA) and Student's *t*-test were carried out for suspended solids at a significance level of $\alpha = 0.05$. The Fisher test results show that F_{cal} is greater than F_{crit} ($F_{cal} = 26.51 > F_{crit} = 4.74$), indicating a statistically significant difference among the groups. The student test results revealed the significance and insignificance parameters by comparing t_{cal} with t_{crit}. When $t_{cal} = t_{crit}$ (2.57), the variable did not influence the response, which helped adjust the model (Equation (11)).

$$SS\ removal(\%) = 73.48 + 12.27X_1 - 19.82X_2 - 8.27X_3 + 8.37X_1X_2 - 5.87X_1X_2X_3 \quad (11)$$

Figure 9 represents the 3D surface plots of suspended solids SS removal as a function of the bed height with the flow rate (Figure 9a), flow rate with time (Figure 9b), and bed height with time (Figure 9c). The bed height had a positive effect of +12.7 on suspended solids removal, with an optimum at +0.33, corresponding to 0.1665m of bed length. The fluid flow and adsorption cycle time had adverse effects on suspended solids removal, with impacts of −19.8 and −8.27, respectively, and an optimum at −1. The negative value of −5.87 for the interaction of the three parameters ($X_1X_2X_3$) indicates a decrease of 5.87% in suspended solids removal at high values of bed height (X_1), flow rate (X_2), and adsorption cycle time (X3), indicating an antagonistic effect and activated carbon saturation. On the other hand, the interaction between bed height (X1) and flow rate (X2) has a positive effect, increasing suspended solids removal by 8.37%.

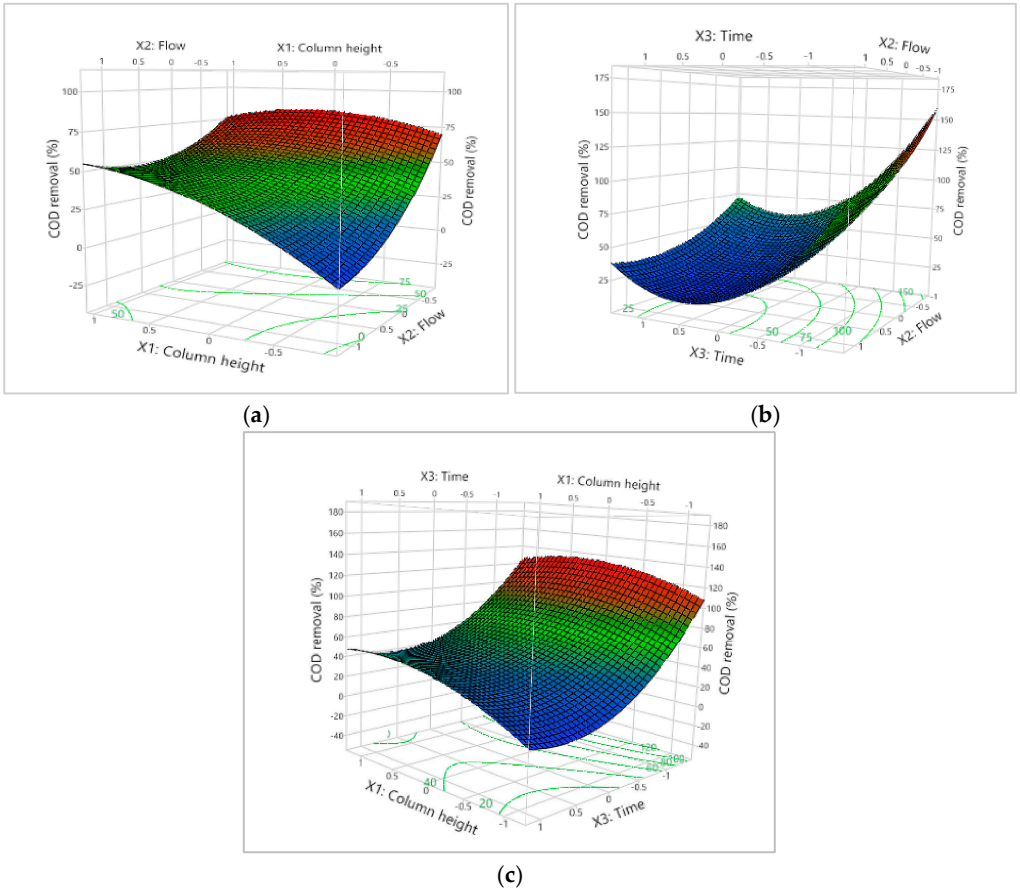

Figure 8. 3D surface plots of COD removal as a function of bed length with the flow (**a**), flow rate with time (**b**), and bed height with time (**c**).

A further simulation was conducted with the optimum values of these three parameters: a bed height of 0.165 m, a feed flow rate of 1 L/h, and an adsorption cycle time of 50 min. The optimisation of elimination rate resulted in 62% and 25% for COD and suspended solids SS respectively, corresponding to an elimination of 81% of the organic and inorganic matter in the solution and 95% of suspended solids. The results agree with Almadani (2023), who found that COD removal increased from 70% to 95% when the bed height was increased from 10 cm to 60 cm, with a higher adsorbent mass and longer contact time [32]. This also aligns with Appiah-Brempong et al. (2024) [52], who observed reduced adsorbed quantity and removal efficiency at higher flow rates (from 2 to 8 mL/min). This led to a drop in the saturation time from 325 to 120 min, and a decrease in COD removal efficiency from 74.60% to 61.54%. Higher flow rates reduced mass transfer

resistance by accelerating the adsorption zone, thereby shortening contaminant residence time and limiting adsorption efficiency. Al-Qodah et al. (2025) [53] similarly showed that increasing bed height improves TOC removal. This is due to a larger adsorbent quantity and a longer contact time, which delays saturation and allows more organic matter to be captured. Likewise, lowering the flow rate increased contact time between water and adsorbent, boosting mass transfer and diffusion within the pores. This resulted in higher TOC removal efficiency and longer column service time.

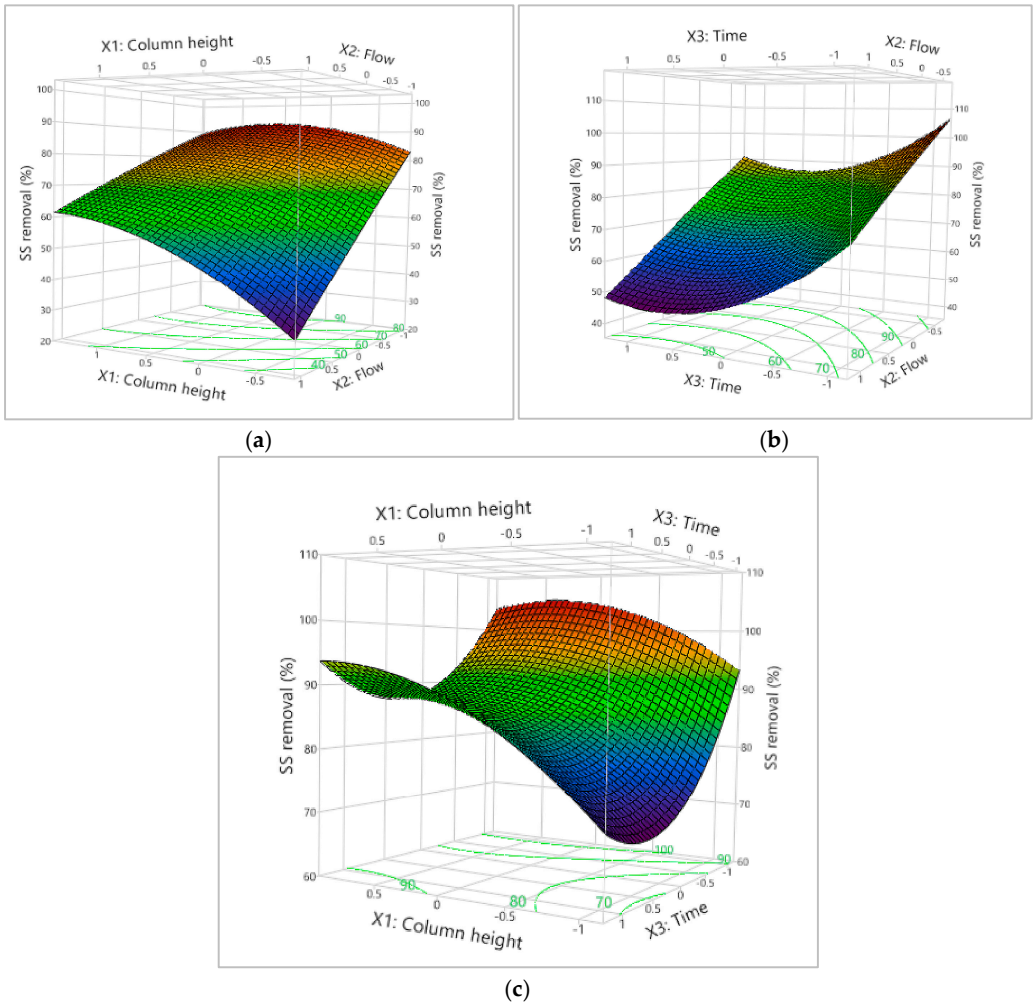

Figure 9. 3D surface plots of SS removal as a function of column height with the flow (**a**), flow rate with time (**b**), and column height with time (**c**).

3.4. Sensitivity Study of Temperature

The effect of temperature was investigated through a case study of COD adsorption behaviour, including kinetics and final separation yield (equilibrium), at 20 °C, 30 °C, and 50 °C was validated by comparison with experimental data from Khellouf's work [36], on the effect of temperature on COD adsorption, using the same activated carbon (characteristics presented in Table 1) and the same textile effluent (characteristics presented in Table 3).

The results confirmed that the activated carbon was not saturated with COD within the first 30 min, as the quantity adsorbed continued to increase linearly over time. At 50 °C, the experimental adsorbed COD after 60 min was 62.5 mg g^{-1}, and the simulated value was 67.7 mg g^{-1}, as shown in Figure 10. At 30 °C, a decrease in adsorbed COD was observed, down to 47.7 mg g^{-1} and 53.1 mg g^{-1}, as indicated by both experimental and

simulation results (Figure 10b). The kinetic relevance increases with the particle mobility at higher collision frequencies, and thermal energy absorption leads to faster diffusion of adsorbate molecules towards the adsorbent surface sites [54,55]. On the other hand, at a temperature of 20 °C and after 60 min of adsorption operation, the adsorbed quantity of COD was approximately equal to that of 50 °C, with both experimental and simulated values reaching 60 mg g^{-1} and 67.2 mg g^{-1}, respectively. The curve of the experimental adsorbed quantity of COD in Figure 10c depicts a slight COD desorption after 23 min of operation. The adsorbed quantity decreased after 60 min of operation, indicating that high temperature increased the mobility of the molecules and, at the same time, activated desorption, thereby reducing separation efficiency and leading to lower adsorbed quantities. The experimentally observed desorption was faster at high temperatures, as illustrated in Figure 10b, where desorption is delayed by 13 min compared to Figure 10c. The numerical model, however, was unable to predict the desorption phenomenon.

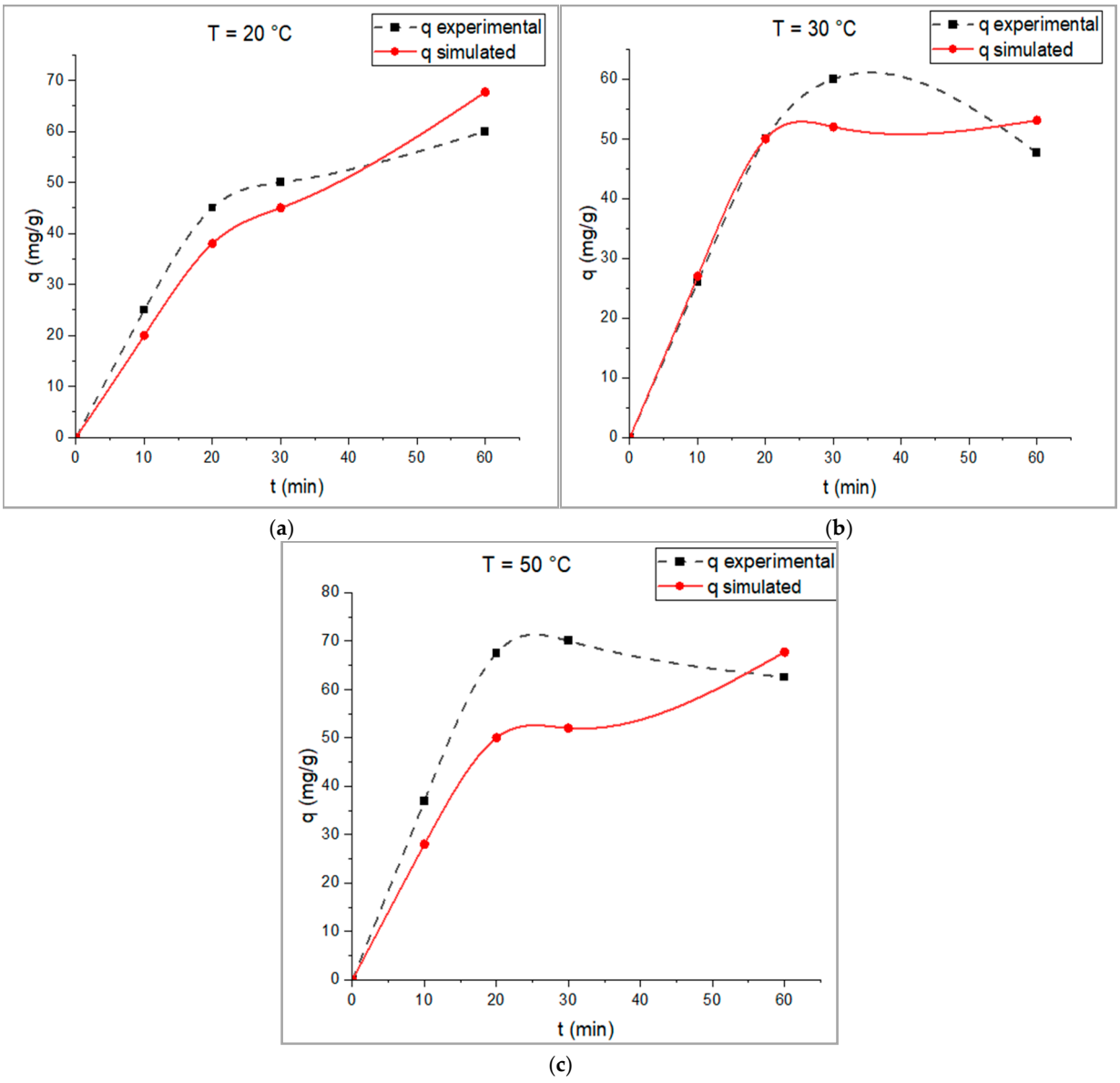

Figure 10. Experimental and simulated adsorbed COD quantities in the textile effluent as a function of time. (**a**) 20 °C, (**b**) 30 °C and (**c**) 50 °C.

4. Conclusions

The mathematical modelling and simulation of effluents from two complex oil and textile industries were performed to predict the effluents' behaviour and contribute to simulate and analyse the dynamic evolution of pollutant indicators, such as COD, suspended solids, and turbidity, during dynamic adsorption on activated carbon derived from mature cypress with a surface area of 379.51 ($m^2.g^{-1}$), and pore volume of 0.204 (cm^3g^{-1}), with the Aspen Plus® adsorption module (Adsim). The simulation results showed good agreement with the experimental data, which proves the applicability of the one-dimensional mathematical model. The results obtained using the numerical tool, based on a coupled equation for mass and heat transport, including a linear approximation of the driving force and reduced heat exchange with the environment, showed that the spatiotemporal variation of the temperature used was slight, less than 1 °C. A simplified 1D mathematical model that neglected the energy equation was therefore feasible in the present study. The relative deviations in concentration ranged from 0.231% to 11.55% for both oil and textile effluents. The investigation of the dynamic process confirmed that several parameters directly influenced molecular diffusion and adsorption profiles. Solid properties, such as density, molecular radius, and molecular weight, affected molecular diffusion in the liquid film and through the pores. Fluid properties, such as density and viscosity, influence molecular diffusion in the liquid phase, thereby affecting adsorption rates. Operating conditions, including temperature, adsorption cycle time, flow rate, and column dimension, directly influenced adsorption efficiency. Flow rate had a negative effect of (−23.34) on COD removal and (−19.82) on suspended solids removal in textile effluent treatment. Both film diffusion and intraparticle diffusion controlled the process.

Complete elimination of the heavy metals (Chromium, Iron, Nickel, and Zinc) was achieved at a bed height of 0.14 m, which corresponded to an elimination rate of 91.5% of suspended solids. At the same time, the chemical oxygen demand (COD) was around 43%. On the other hand, elimination rates of 71.31%,83% and 80.4% for suspended solids, TOC and colour reduction, respectively, and 19% for the chemical oxygen demand were observed in the textile effluent treatment, with saturation in some heavy metals (Manganese and Cadmium), suggesting that current operating conditions are insufficient for effective treatment of textile effluent. The optimisation of the relevant parameters for treating textile effluent was carried out using response surface methodology with a central composite design. The column performance was achieved with elimination rates of 62% for COD and 25% for suspended solids. These promising indicators of separation will be considered for a stepwise extension of both laboratory data and simulations in a pilot plant, where the relevance of fluid flow, mass, and heat transfer is greater. The applicability of the assumptions made in the work will be adjusted accordingly.

These results highlight the need for further research into the complex interplay between ion size, charge density, and hydration effects on adsorption site occupancy and overall process efficiency. A key future direction involves scaling up the fixed-bed column to more realistic operating conditions that better represent industrial-scale applications. The current literature remains limited, particularly with respect to the physical properties of complex aqueous matrices and sorbent materials when described using deterministic or data-driven approaches. Integrating advanced modelling frameworks, including machine learning techniques, offers a promising approach to handling large datasets and capturing mutual interactions that are difficult to model with classical methods such as those employed in this study.

At larger scales, increased turbulence, complex flow structures, and local hydrodynamic instabilities can significantly reduce the validity of simple linear scale-up correlations. These challenges will be mitigated by adding experimental studies to the coupled model, along with advanced three-dimensional computational fluid dynamics models to better capture flow non-uniformities and mass transfer limitations.

Author Contributions: Conceptualization, S.R., R.C., G.S. and F.A.; methodology, S.R., R.C., G.S. and F.A.; software, S.R., G.S. and F.A.; validation, S.R., R.C., G.S. and F.A.; formal analysis, S.R., R.C., G.S. and F.A.; investigation, S.R., R.C., G.S. and F.A.; data curation, S.R., R.C., G.S. and F.A.; writing—original draft preparation, S.R., R.C., G.S. and F.A.; writing—review and editing, S.R., R.C., G.S. and F.A.; visualization, S.R., G.S. and F.A.; supervision, R.C., G.S. and F.A.; project administration, R.C.; funding acquisition, R.C. All authors have read and agreed to the published version of the manuscript.

Funding: This research received no external funding.

Data Availability Statement: The original contributions presented in this study are included in the article. Further inquiries can be directed to the corresponding author.

Conflicts of Interest: The authors declare no conflict of interest.

Abbreviations

A	cross-sectional area of the packed bed (m^2)
c_i	bulk concentration of species i in the fluid phase (mol m^{-3})
c_i^*	equilibrium concentration of species i in the fluid phase (mol m^{-3})
$c_{p,i}$	specific heat capacity of the adsorbed species i or solid phase (J $kg^{-1}K^{-1}$)
$c_{p,li}$	specific heat capacity of the liquid phase (J kg^{-1} K^{-1})
D_{ei}	effective axial dispersion coefficient of species i in the packed bed (m^2 s^{-1})
D_{eff}	effective diffusivity of species i within the solid or porous phase (m^2 s^{-1})
D_{mi}	molecular diffusivity of species i in the fluid phase (m^2 s^{-1})
D_{SO}	limiting or intrinsic surface diffusivity of species i at infinite dilution (m^2 s^{-1})
K	Boltzmann constant (1.3806×10^{-23} J K^{-1})
k	effective axial thermal conductivity of the packed bed (W m^{-1} K^{-1})
k_{LDF}	linear driving force mass transfer coefficient (s^{-1})
q_i^*	equilibrium adsorbed concentration of species i on the solid phase (mol kg^{-1} of solid)
q_i	instantaneous adsorbed concentration of species i (mol kg^{-1} of solid)
$\bar{q}_i$	volume-averaged adsorbed concentration within the particle (mol kg^{-1} of solid)
r_i	hydrodynamic radius of species i (m)
r_p	radius of the adsorbent particle (m)
T	absolute temperature (K)
t	time (s)
ΔT	temperature difference relative to the reference temperature, $T - T_{ref}$ (K)
U	superficial fluid velocity (m s^{-1})
V_v	void (interstitial) volume of the adsorption column (m^3)
z	axial coordinate along the column height (m)
ε	bed porosity (-)
Sh_i	Sherwood number for species i (-)
ε_p	intraparticle porosity of the adsorbent (-)
ρ_p	particle density of the adsorbent (kg m^{-3})
μ_f	dynamic viscosity of the fluid (Pa s)
ρ_l	density of the liquid phase (kg m^{-3})
$\Delta H_{ads,i,T_{ref}}$	heat of adsorption of species i evaluated at reference temperature T_{ref} (J mol^{-1})
ρ_i	density of the adsorbed phase or solid associated with species i (kg m^{-3})

References

1. Castillo-Suárez, L.A.; Sierra-Sánchez, A.G.; Linares-Hernández, I.; Martínez-Miranda, V.; Teutli-Sequeira, E.A. A critical review of textile industry wastewater: Green technologies for the removal of indigo dyes. *Int. J. Environ. Sci. Technol. IJEST* **2023**, *20*, 10553–10590. [CrossRef] [PubMed]
2. Thombre, N.; Patil, P.; Yadav, A.; Patwardhan, A. A short review on water management and reuse in textile industry—A sustainable approach. *Discov. Water* **2025**, *5*, 26. [CrossRef]
3. Alkhazraji, H.; Alatabe, M.J.A. Coagulation/flocculation process for oily wastewater treatment. *J. Eng. Sustain. Dev.* **2021**, *25*, 3–68. [CrossRef]
4. Onyena, A.P.; Sam, K. A review of the threat of oil exploitation to mangrove ecosystem: Insights from Niger Delta, Nigeria. *Glob. Ecol. Conserv.* **2020**, *22*, e00961. [CrossRef]
5. Sharma, K.; Shah, G.; Singhal, K.; Soni, V. Comprehensive insights into the impact of oil pollution on the environment. *Reg. Stud. Mar. Sci.* **2024**, *74*, 103516. [CrossRef]
6. Rana, S.; Verma, Y. Biochemical toxicity of benzene. *J. Environ. Biol.* **2005**, *26*, 157–168.
7. Ahmad Khan, H. Short Review: Benzene's toxicity: A consolidated short review of human and animal studies. *Hum. Exp. Toxicol.* **2007**, *26*, 677–685. [CrossRef]
8. Balachandran, B.; Sabumon, P.C. A comprehensive review on biodegradation of azo dye mixtures, metabolite profiling with health implications and removal strategies. *J. Hazard. Mater. Adv.* **2025**, *19*, 100834. [CrossRef]
9. Georgiou, D.; Melidis, P.; Aivasidis, A.; Gimouhopoulos, K. Degradation of azo-reactive dyes by ultraviolet radiation in the presence of hydrogen peroxide. *Dye. Pigment.* **2002**, *52*, 69–78. [CrossRef]
10. Berez, A.; Schäfer, G.; Ayari, F.; Trabelsi-Ayadi, M. Adsorptive removal of azo dyes from aqueous solutions by natural bentonite under static and dynamic flow conditions. *Int. J. Environ. Sci. Technol.* **2016**, *13*, 1625–1640. [CrossRef]
11. Manzoor, D.; Sharma, M. *Impact of Textile Dyes on Human Health and Environment*; Jiwaji University: Gwalior, India, 2020; pp. 162–169. [CrossRef]
12. Meryem, K.; Chemini, R.; Salem, Z.; Khodja, M.; Zeriri, D. Parametric Study of COD Reduction from Textile Processing Wastewater Using Adsorption on Cypress Cone-Based Activated Carbon: An Analysis of a Doehlert Response Surface Design. *Arab. J. Sci. Eng.* **2019**, *44*, 10079–10086. [CrossRef]
13. Lu, J.; Zhou, Y.; Liu, Y. Recent advances for dyes removal using novel adsorbents: A review. *Environ. Pollut.* **2019**, *252*, 352–365. [CrossRef] [PubMed]
14. Liu, Y.; Chen, Q.; Singh, R. Low-Cost RSAC and Adsorption Characteristics in the Removal of Copper Ions from Wastewater. *Appl. Sci.* **2022**, *12*, 5612. [CrossRef]
15. Titchou, F.; Hicham, Z.; Hanane, A.; El Gaayda, J.; Akbour, R.; Hamdani, M. Removal of Persistent Organic Pollutants (POPs) from Water and Wastewater by Adsorption and Electrocoagulation Process. *Groundw. Sustain. Dev.* **2021**, *13*, 100575. [CrossRef]
16. Yıldız Töre, G.; Meric, S.; Lofrano, G.; De Feo, G. Removal of Trace Pollutants from Wastewater in Constructed Wetlands. In *Emerging Compounds Removal from Wastewater: Natural and Solar Based Treatments*; Lofrano, G., Ed.; Springer: Dordrecht, The Netherlands, 2012; pp. 39–58. [CrossRef]
17. Pongwiwanna, D.; Tangsathitkulchai, C. The Use of High Surface Area Mesoporous-Activated Carbon from Longan Seed Biomass for Increasing Capacity and Kinetics of Methylene Blue Adsorption from Aqueous Solution. *Molecules* **2021**, *26*, 6521. [CrossRef]
18. Azam, K.; Shezad, N.; Shafiq, I.; Akhter, P.; Akhtar, F.; Jamil, F.; Shafique, S.; Park, Y.-K.; Hussain, M. A review on activated carbon modifications for the treatment of wastewater containing anionic dyes. *Chemosphere* **2022**, *306*, 135566. [CrossRef]
19. Kallawar, G.A.; Bhanvase, B.A. A review on existing and emerging approaches for textile wastewater treatments: Challenges and future perspectives. *Environ. Sci. Pollut. Res. Int.* **2024**, *31*, 1748–1789. [CrossRef]
20. Malloum, A.; Adegoke, K.A.; Ighalo, J.O.; Conradie, J.; Ohoro, C.R.; Amaku, J.F.; Oyedotun, K.O.; Maxakato, N.W.; Akpomie, K.G.; Okeke, E.S.; et al. Computational methods for adsorption study in wastewater treatment. *J. Mol. Liq.* **2023**, *390*, 123008. [CrossRef]
21. Simo, M.; Brown, C.J.; Hlavacek, V. Simulation of pressure swing adsorption in fuel ethanol production process. *Comput. Chem. Eng.* **2008**, *32*, 1635–1649. [CrossRef]
22. Jribi, S.; Miyazaki, T.; Saha, B.B.; Koyama, S.; Maeda, S.; Maruyama, T. Corrected adsorption rate model of activated carbon–ethanol pair by means of CFD simulation. *Int. J. Refrig.* **2016**, *71*, 60–68. [CrossRef]
23. Jribi, S.; Miyazaki, T.; Saha, B.B.; Koyama, S.; Maeda, S.; Maruyama, T. CFD simulation and experimental validation of ethanol adsorption onto activated carbon packed heat exchanger. *Int. J. Refrig.* **2017**, *74*, 345–353. [CrossRef]
24. Bhatt, T.; Storti, G.; Rota, R. Detailed simulation of dual-reflux pressure swing adsorption process. *Chem. Eng. Sci.* **2015**, *122*, 34–52. [CrossRef]
25. Santos, M.G.R.S.; Correia, L.M.S.; de Medeiros, J.L.; Araújo, O.d.Q.F. Natural gas dehydration by molecular sieve in offshore plants: Impact of increasing carbon dioxide content. *Energy Convers. Manag.* **2017**, *149*, 760–773. [CrossRef]

26. Bahrun, M.H.V.; Bono, A.; Othman, N.; Zaini, M.A.A. Numerical modelling and simulation of methane enrichment: A systematic review on pressure swing adsorption technology. *Int. J. Model. Simul.* **2024**, 1–39. [CrossRef]
27. Xu, Z.; Cai, J.-g.; Pan, B.-c. Mathematically modeling fixed-bed adsorption in aqueous systems. *J. Zhejiang Univ. Sci. A* **2013**, *14*, 155–176. [CrossRef]
28. Leonavičienė, T.; Ciegis, R.; Baltrėnaitė-Gedienė, E.; Chemerys, V. Numerical analysis of liquid-solid adsorption model. *Math. Model. Anal.* **2019**, *24*, 598–616. [CrossRef]
29. Rodríguez-Narciso, S.; Lozano-Álvarez, J.A.; Salinas-Gutiérrez, R.; Castañeda-Leyva, N. A Stochastic Model for Adsorption Kinetics. *Adsorpt. Sci. Technol.* **2021**, *2021*, 5522581. [CrossRef]
30. Liu, L. A comprehensive model of adsorption of resorcinol in rotating packed bed: Theoretical, isotherm, kinetics and thermodynamics. *J. Environ. Chem. Eng.* **2023**, *11*, 111041. [CrossRef]
31. Malloum, A.; Akpotu, S.O.; Adegoke, K.A.; Okeke, E.S.; Omotola, E.O.; Ohoro, C.R.; Amaku, J.F.; Conradie, J.; Olisah, C.; Akpomie, K.G. Advances in molecular simulations of dye adsorption from wastewater. *J. Mol. Liq.* **2025**, *439*, 128732. [CrossRef]
32. Almadani, M. Adsorption process modeling to reduce COD by activated carbon for wastewater treatment. *Chemosphere* **2023**, *339*, 139691. [CrossRef]
33. Bencheikh, I.; Azoulay, K.; Samghouli, N.; Mabrouki, J.; Bouhachlaf, L.; Moufti, A.; El Hajjaji, S. Mathematical and Statistical Study for the Wastewater Adsorbent Regeneration Using the Central Composite Design. In *IoT and Smart Devices for Sustainable Environment*; Azrour, M., Irshad, A., Chaganti, R., Eds.; Springer International Publishing: Cham, Switzerland, 2022; pp. 71–83. [CrossRef]
34. Sukriti; Sharma, J.; Pruthi, V.; Anand, P.; Singh Chaddha, A.P.; Bhatia, J.; Kaith, B.S. Surface response methodology–central composite design screening for the fabrication of a Gx-psy-g-polyacrylicacid adsorbent and sequestration of auramine-O dye from a textile effluent. *RSC Adv.* **2016**, *6*, 74300–74313. [CrossRef]
35. Nair, A.T.; Makwana, A.; Ahammed, M. The use of response surface methodology for modelling and analysis of water and wastewater treatment processes: A review. *Water Sci. Technol. A J. Int. Assoc. Water Pollut. Res.* **2014**, *69*, 464–478. [CrossRef]
36. Khellouf, M. Optimization of a Hybrid Process for Treatment of Polluted Water. Application to Hydrocarbons and Colorants. Ph.D. Thesis, University of Science and Technology Houari Boumediene, Algiers, Algeria, 2020. Available online: https://dspace.usthb.dz/items/f3a85feb-63c2-4852-bbe5-1fcc644b359d (accessed on 24 May 2021).
37. Khellouf, M.; Chemini, R.; Salem, Z.; Khodja, M.; Zeriri, D.; Jada, A. A new activated carbon prepared from cypress cones and its application in the COD reduction and colour removal from industrial textile effluent. *Environ. Dev. Sustain.* **2021**, *23*, 7756–7771. [CrossRef]
38. Bear, J. *Dynamics of Fluids in Porous Media*; American Elsevier Publishing Company: New York, NY, USA, 1972.
39. Guelli Souza, S.; Peruzzo, L.; Souza, A. Numerical study of the adsorption of dyes from textile effluents. *Appl. Math. Model.* **2008**, *32*, 1711–1718. [CrossRef]
40. Shafeeyan, M.S.; Daud, W.; Shamiri, A. A review of mathematical modeling of fixed-bed columns for carbon dioxide adsorption. *Chem. Eng. Res. Des.* **2014**, *92*, 961–988. [CrossRef]
41. Tavan, Y.; Hosseini, S.H.; Ahmadi, G.; Olazar, M. Mathematical model and Energy Analysis of Ethane Dehydration in a Two-layer Packed Bed Adsorption. *Particuology* **2018**, *47*, 33–40. [CrossRef]
42. El-Sharkawy, I. On the linear driving force approximation for adsorption cooling applications. *Int. J. Refrig.* **2011**, *34*, 667–673. [CrossRef]
43. Lee, J.-J.; Kim, M.-K.; Lee, D.-G.; Ahn, H.; Kim, M.-J.; Lee, C.-H. Heat-exchange pressure swing adsorption process for hydrogen separation. *AIChE J.* **2008**, *54*, 2054–2064. [CrossRef]
44. Edwards, M.F.; Richardson, J.F. Gas dispersion in packed beds. *Chem. Eng. Sci.* **1968**, *23*, 109–123. [CrossRef]
45. Ge, X.-H.; Jia, B.; Shan, Z.; Lin, X.; Wang, X. The overall-process dynamic mass transfer research of surfactant at the three-phase emulsions interface. *AIChE J.* **2025**, *71*, e18716. [CrossRef]
46. Satyam, S.; Patra, S. Innovations and challenges in adsorption-based wastewater remediation: A comprehensive review. *Heliyon* **2024**, *10*, e29573. [CrossRef]
47. Długosz, O.; Banach, M. Sorption of Ag+ and Cu^{2+} by Vermiculite in a Fixed-Bed Column: Design, Process Optimization and Dynamics Investigations. *Appl. Sci.* **2018**, *8*, 2221. [CrossRef]
48. Hu, Q.; Wang, D.; Pang, S.; Xu, L. Prediction of breakthrough curves for multicomponent adsorption in a fixed-bed column using logistic and Gompertz functions. *Arab. J. Chem.* **2022**, *15*, 104034. [CrossRef]
49. Benmahdi, F.; Semra, S.; Haddad, D.; Mandin, P.; Kolli, M.; Bouhelassa, M. Breakthrough Curves Analysis and Statistical Design of Phenol Adsorption on Activated Carbon. *Chem. Eng. Technol.* **2018**, *42*, 355–369. [CrossRef]
50. Csempesz, F.; Csáki, K.F. Conformational changes induced by competitive adsorption in mixed interfacial layers of uncharged polymers. In *Studies in Surface Science and Catalysis*; Iwasawa, Y., Oyama, N., Kunieda, H., Eds.; Elsevier: Amsterdam, The Netherlands, 2001; Volume 132, pp. 275–278. [CrossRef]

51. Bayuo, J.; Rwiza, M.; Sillanpää, M.; Mtei, K. Removal of heavy metals from binary and multicomponent adsorption systems using various adsorbents—A systematic review. *RSC Adv.* **2023**, *13*, 13052–13093. [CrossRef]
52. Appiah-Brempong, M.; Essandoh, H.M.K.; Asiedu, N.Y.; Momade, F.Y. Bone Char Adsorption of COD and Colour from Tannery Wastewater: Breakthrough Curve Analysis and Fixed Bed Dynamic Modelling. *Adv. Civ. Eng.* **2024**, *2024*, 6651094. [CrossRef]
53. Al-Qodah, Z.; Al-Shannag, M.; Hudaib, B.; Bani-Salameh, W.; Shawaqfeh, A.T.; Assirey, E. Synergy and enhanced performance of combined continuous treatment processes of pre-chemical coagulation (CC), solar-powered electrocoagulation (SAEC), and post-adsorption for Dairy wastewater. *Case Stud. Chem. Environ. Eng.* **2025**, *11*, 101183. [CrossRef]
54. Wang, C.; Myshkin, V.; Khan, V.; Poberezhnikov, A.; Baraban, A. Effect of Temperature on the Diffusion and Sorption of Cations in Clay Vermiculite. *ACS Omega* **2022**, *7*, 11596–11605. [CrossRef]
55. Xie, Z.; Xiao, L.; Luo, S.; Liao, G. Numerical simulation study on the effect of temperature on the restricted diffusion in porous media. *Magn. Reson. Lett.* **2023**, *3*, 118–126. [CrossRef]